PHYSICAL REVIEW D **93,** 054509 (2016)

ρ and K^* resonances on the lattice at nearly physical quark masses and $N_f = 2$

Gunnar S. Bali,[1,2] Sara Collins,[1] Antonio Cox,[1] Gordon Donald,[1] Meinulf Göckeler,[1] C. B. Lang,[3] and Andreas Schäfer[1]
(RQCD Collaboration)

[1]*Institute for Theoretical Physics, University of Regensburg, 93040 Regensburg, Germany*
[2]*Tata Institute of Fundamental Research, Homi Bhabha Road, Mumbai 400005, India*
[3]*Institute of Physics, University of Graz, A-8010 Graz, Austria*
(Received 1 January 2016; published 22 March 2016)

Working with a pion mass $m_\pi \approx 150$ MeV, we study $\pi\pi$ and $K\pi$ scattering using two flavors of nonperturbatively improved Wilson fermions at a lattice spacing $a \approx 0.071$ fm. Employing two lattice volumes with linear spatial extents of $N_s = 48$ and $N_s = 64$ points and moving frames, we extract the phase shifts for p-wave $\pi\pi$ and $K\pi$ scattering near the ρ and K^* resonances. Comparing our results to those of previous lattice studies, that used pion masses ranging from about 200 MeV up to 470 MeV, we find that the coupling $g_{\rho\pi\pi}$ appears to be remarkably constant as a function of m_π.

DOI: 10.1103/PhysRevD.93.054509

I. INTRODUCTION

Lattice QCD calculations are particularly suited for studies of hadrons which are stable under the strong interaction and their properties can be determined by studying correlation functions at large Euclidean time separations. However, almost all known hadrons are unstable resonances, which complicates the situation. The ρ meson, one of the simplest resonances in QCD, couples to a pair of pions with total isospin $I = 1$. In a finite lattice volume of linear spatial size $L = N_s a$, the allowed momenta of the pion pair are quantized. Neglecting $\pi\pi$ interactions, the lowest-lying $\pi\pi$ state with the same spin $J = 1$ as the ρ has the energy

$$E_{\pi\pi}^{\text{free}} = 2\sqrt{m_\pi^2 + \left(\frac{2\pi}{L}\right)^2}. \tag{1}$$

The ρ can only be treated as a stable particle if its mass is sufficiently smaller than this $\pi\pi$ center-of-momentum-frame energy $E_{\pi\pi}^{\text{free}}$. This is possible if the pion is heavy or the lattice size is small. For the values of m_π and L that are now accessible in lattice simulations this is not the case anymore.

The formalism for dealing with resonances in lattice QCD simulations of two-particle scattering systems has been developed first with equal masses and in systems at rest [1,2] and later extended to various moving frames and unequal masses [3–10]. In $\pi\pi$ scattering, the ρ appears as an increase of the scattering phase shift from zero to π as the center-of-momentum-frame energy, E_{cm}, is varied from below to above the resonant mass value m_ρ. The dependence of the $\ell = 1$ angular momentum partial wave shift δ on E_{cm} gives detailed information about the nature of the resonance. To first approximation, the resonant mass can be extracted at the value $\delta = \pi/2$.

Due to the computational cost, previous calculations of the resonance parameters were restricted to unphysically large pion masses (most even employed pion masses with $E_{\pi\pi}^{\text{free}} > m_\rho$), but the expected phase-shift behavior was still observed [6,11–20]. Algorithmic advances and increases in computer power now enable us to pursue the first scattering study at a close to physical pion mass $m_\pi \approx 150$ MeV.

The strange-light analogue of the light-light ρ meson is the K^*. Its phase shift has also been studied previously in lattice calculations at unphysically large pion masses [21–24]. There are similarities between $\pi\pi$ and $K\pi$ scattering not only in terms of the formalism but also in terms of constructing and computing the necessary correlation functions, which means we can incorporate the K^* resonance into our study, with limited computational overhead.

From experiment, the ρ has a mass of around 775 MeV and a decay width $\Gamma_\rho \approx 148$ MeV while the K^* mass and width are approximately 896 and 47 MeV [25], respectively. The decays are almost exclusively to $\pi\pi$ and $K\pi$. In our study of the ρ resonance we neglect couplings to three- and four-pion states. Our calculation (and all other $\pi\pi$ scattering calculations to date) is performed with isospin symmetry in place, and therefore 3π final states are excluded. Isospin symmetry tremendously simplifies the computation for the $I = 1$ ρ and the $I = 1/2$ K^* channels we consider here as there are no disconnected quark-line contractions. As we will see, at our pion mass and for the kinematics we implement, only one of our data points could be sensitive to 4π final states. Also, considering the available phase space and Okubo-Zweig-Iizuka suppression, neglecting these multiparticle final states should be a very good approximation. This argument is supported by

TABLE I. Details of the lattice configurations: volume, coupling, lattice spacing (determined in Ref. [31]), light and strange quark mass parameters κ_ℓ and κ_s, (finite-volume) pion mass, kaon mass, the linear spatial size in units of the infinite-volume pion mass Lm_π^∞ [32], the unit momentum $2\pi/L$ and the number of configurations $N_{\rm cfg}$ analyzed. The errors given for m_π and m_K are statistical only and do not include the 3% scale-setting uncertainty [31].

$N_s^3 \times N_t$	β	a^{-1}	κ_ℓ	κ_s	m_π	m_K	Lm_π^∞	$2\pi/L$	$N_{\rm cfg}$
$48^3 \times 64$	5.29	2.76(8) GeV	0.13640	0.135574	160(2) MeV	500(1) MeV	2.61	361 MeV	888
$64^3 \times 64$	5.29	2.76(8) GeV	0.13640	0.135574	150(1) MeV	497(1) MeV	3.48	271 MeV	671

experimental evidence, indeed suggesting a virtually undetectable coupling of the ρ meson to 4π states [26]. Comparing measurements of the branching fractions of $\rho \to 4\pi$ and the (isospin-breaking) $\rho \to 3\pi$ decay [26,27] shows that they are of similar (small) sizes. For a neutral ρ meson, the decay width to $\pi^+\pi^-\pi^0$ is 15(7) keV. Combining the widths to $\pi^+\pi^-\pi^0\pi^0$ and $\pi^+\pi^-\pi^+\pi^-$ gives 5(2) keV. This is indeed negligible, relative to the total width of 148 MeV. For decays of a charged ρ into four pions only an upper limit exists.

In the cases of $\pi\pi$ and $K\pi$ scattering, respectively, in principle there could also be interference with $K\bar{K}$ and $K\eta$; $2m_K \approx 985$ MeV, $m_K + m_\eta \approx 1040$ MeV. However, both values are well above the region we are interested in, in particular considering p-wave decay in a finite volume. For heavier-than-physical pions, these thresholds are closer. This situation was studied at $m_\pi \approx 236$ MeV in Ref. [18] for the ρ resonance and at $m_\pi \approx 391$ MeV in Ref. [24] for the K^*. Indeed, even at these large pion masses, the impact was found to be negligible. Finally, we also ignore $K^* \to K\pi\pi$, noting that the upper limit reads $\Gamma(K^* \to K\pi\pi) \approx 35$ keV [28]; the vast majority of experimentally observed decays to $K\pi\pi$ final states appear to be related to heavier resonances [29].

Our method to generate the necessary correlation functions has been employed in previous calculations [6,11,14]. Nevertheless, we provide a brief description of the construction of correlators, along with details on the lattices and kinematics used in Sec. II. The results are presented and discussed in Sec. III, before we conclude in Sec. IV.

II. LATTICE CALCULATION

We aim to extract the resonance parameters (mass and width) of the ρ and K^* from their appearances in $\pi\pi$ and $K\pi$ p-wave scattering, respectively. To do so, we will determine the spectra of interacting two-particle QCD states in finite volumes. Using these energy levels, along with known relations, allows us to extract the scattering phase shift, from whose dependence on the energy $E_{\rm cm}$ in the rest frame of the ρ (or the K^*) the resonance parameters can be found.

A. Discussion of the lattice parameters

We employ lattice configurations with a lattice spacing $a \approx 0.071$ fm and time extent $N_t a = 64a \approx 4.6$ fm, generated by the Regensburg lattice QCD group (RQCD, $L = 64a$) and RQCD/QCDSF ($L = 48a$) with $N_f = 2$ flavors of degenerate nonperturbatively improved Wilson sea quarks with a pion mass of about 150 MeV (ensembles VIII and VII of Ref. [30]). On the larger volume every second trajectory and on the smaller volume every fifth trajectory is analyzed. Discretization errors are of $\mathcal{O}(a^2)$. We expect these to be small for the light hadron masses considered at our lattice scale $a^{-1} = 2.76(8)$ GeV [31]. The lattice parameters are given in Table I. More detail can be found in Refs. [30,32]. Following Ref. [33], we check the strange quark mass tuning by computing $\sqrt{2m_K^2 - m_\pi^2} = 686.5(1.1)$ MeV on the $N_s = 64$ ensemble, assuming $a^{-1} = 2.76$ GeV. We find perfect agreement with the "experimental" value of 686.9 MeV.

The choice of our ensembles is motivated by the proximity of the pion mass to its experimental value. In the $\rho \to \pi\pi$ channel the pions must have relative angular momentum. For a system at rest this is only possible if their individual momenta are nonzero. This gives the threshold (1), where $m_\rho > E_{\rm cm}^{\rm free} > 2m_\pi$, for the ρ to become unstable in a finite volume. On our lattice configurations, this threshold lies at 782 MeV (within the experimental ρ resonance width) for $N_s = 48$ and at 619 MeV (beneath the resonance) for $N_s = 64$. Note that in moving frames the effective thresholds can be lower.

The combination Lm_π is the relevant quantity controlling finite-size effects. This combination obviously decreases with m_π and it is expensive to enlarge the linear box size L to fully compensate for this. Our lattice volumes have $Lm_\pi < 4$, due to limited computer resources. However, there are clear advantages to employ small volumes for resolving broad resonances like the ρ: at large L the spectrum of two-particle states becomes dense, complicating the extraction of the relevant energy levels and increasing the demand on the precision of their determination.

Terms which are exponentially suppressed in Lm_π are neglected in the Lüscher phase-shift method [1]. One such effect is the difference between the pion mass $m_\pi \approx 160$ MeV on the small volume and its infinite-volume value $m_\pi^\infty \approx 149.5$ MeV [30], which goes beyond this formalism. Note that $Lm_\pi^\infty \approx 2.6$ for our smaller volume and $e^{-2.6} \approx 0.074$ may not necessarily be considered a small number. Fortunately, it has been demonstrated, at least in some models, e.g., in the inverse amplitude and the N/D_A models, that for $I = 1$ p-wave $\pi\pi$ scattering the

corrections to the Lüscher formula may be negligible as long as $Lm_\pi > 2$ [34]. We note that towards small pion masses the ρ resonance broadens, allowing us to extract nontrivial phase shifts for a wider range of energies than had been possible in previous simulations at unphysically large pion masses. This allows us to collect several data points within the region relevant to constrain the resonance parameters.

An issue that arises for pions which are sufficiently close to their physical mass is the opening of the four-pion threshold as, in nature, $m_\rho > 4m_\pi$. In analogy to our discussion of two-particle thresholds, we can determine where the four-particle thresholds will lie for the lattice configurations we use. When the ρ meson is at rest at least two of the pions need to carry nonzero momenta. In this case, a decay to four pions requires 918 MeV on our larger lattice size and 1081 MeV on the smaller one, both of which lie well above the resonance region.

Again, for moving frames, these limits can be lower. We encounter the worst case for the total momentum $\mathbf{P} = (0,0,1)(2\pi/L)$ on $L = 64a$, where the four-pion threshold lies around $E_{\rm cm} = 710$ MeV. Fortunately, as we discussed in the Introduction, the ρ and K^* resonances are entirely dominated by p-wave decays into $\pi\pi$ and $K\pi$ final states; even in experiment other channels are hardly detectable at all. Finally, we remark that dealing with decays to more than two particles in lattice QCD is an open problem. While there has been recent theoretical progress addressing three-particle final states [35–39], we do not know how to analyze four-pion states in a lattice calculation.

B. Generation of the correlators

In order to treat the ρ as a resonance in $\pi\pi$ scattering, we employ a basis of interpolators which explicitly couple to one- and two-particle states. The interpolators used for each kinematic setting all share the same quantum numbers and symmetries. In the case of $\pi\pi$ scattering, we are interested in the $I = 1$, $J^P = 1^-$ channel in which the ρ appears. The $\pi\pi$ interpolators read

$$\pi(\mathbf{p}_1)\pi(\mathbf{p}_2) = \frac{1}{\sqrt{2}}[\pi^+(\mathbf{p}_1)\pi^-(\mathbf{p}_2) - \pi^-(\mathbf{p}_1)\pi^+(\mathbf{p}_2)], \quad (2)$$

where $\pi = \bar\psi\gamma_5\psi$ and the one-particle vector interpolator has the momentum $\mathbf{P} = \mathbf{p}_1 + \mathbf{p}_2$. For this we use three structures in our basis: $\bar\psi\gamma_j\psi$, $\bar\psi\gamma_j\gamma_t\psi$ and $\bar\psi\nabla_j\psi$.

We apply Wuppertal quark smearing [40], where the field, $\phi_x^{(n)}$, at site x after n smearing iterations is

$$\phi_x^{(n)} = \frac{1}{1+6\delta}\left(\phi_x^{(n-1)} + \delta\sum_{j=\pm1}^{\pm3} U_{x,j}\phi_{x+a\hat\jmath}^{(n-1)}\right). \quad (3)$$

We set $\delta = 0.25$ and employ three levels of quark smearing, using 50, 100 or 150 iterations. $U_{x,\mu}$ is a (smeared) gauge link connecting x with $x + a\hat\mu$ and $U_{x,-\mu} = U^\dagger_{x-a\hat\mu,\mu}$. For the pseudoscalar meson operators, we choose the narrowest smearing width. We use all three smearing levels for $\bar\psi\gamma_j\psi$ and $\bar\psi\gamma_j\gamma_t\psi$ and only the narrowest for $\bar\psi\nabla_j\psi$, so we have one two-particle interpolator and a total of seven one-particle interpolators. We employ spatial APE smearing for the gauge links [41] that appear within Eq. (3) above:

$$U_{x,i}^{(n)} = P_{\rm SU(3)}\left(\alpha U_{x,i}^{(n-1)} + \sum_{|j|\neq i} U_{x,j}^{(n-1)} U_{x+a\hat\jmath,i}^{(n-1)} U_{x+a\hat\imath,j}^{(n-1)\dagger}\right) \quad (4)$$

with $i \in \{1,2,3\}$, $j \in \{\pm1,\pm2,\pm3\}$. $P_{\rm SU(3)}$ denotes a projection into the SU(3) group. We use $\alpha = 2.5$ and 25 iterations.

In $K\pi$ scattering, the K^* resonance is in the $I = 1/2$ channel, so we use

$$\pi(\mathbf{p}_1)K(\mathbf{p}_2) = \sqrt{\frac{2}{3}}\pi^+(\mathbf{p}_1)K^-(\mathbf{p}_2) - \sqrt{\frac{1}{3}}\pi^0(\mathbf{p}_1)K^0(\mathbf{p}_2) \quad (5)$$

as the two-particle interpolator. The one-particle interpolators are the same as for the ρ resonance, replacing one light quark by the strange. From these interpolators we calculate a matrix of correlation functions. The contractions for its entries are depicted in Fig. 1.

By using the two volumes and a number of moving frames, we are able to access several points within the regions of interest around the expected positions of the ρ and K^* resonances. The kinematic points we use are given in Table II, where

$$\mathbf{K} = \frac{L}{2\pi}\mathbf{P} \quad (6)$$

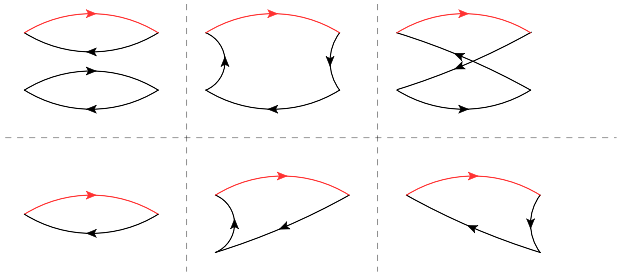

FIG. 1. Diagrams showing the quark contractions for the entries of our correlation matrices for $\pi\pi$ and $K\pi$ scattering. The red propagator denotes a strange quark for $K\pi$ and a light one for $\pi\pi$, while the black propagators are for light quarks in both cases. The top row shows contractions for $2 \to 2$ particle correlators. The rightmost diagram does not appear for $I = 1$ $\pi\pi$ scattering, but is required for our $K\pi$ scattering calculation. The second row contains $1 \to 1$, $2 \to 1$ and $1 \to 2$ entries, respectively, where the $1 \to 2$ element is the complex conjugate of $2 \to 1$.

TABLE II. The interpolators we use in different moving frames. For each frame, we note the little group and irreducible representations (irrep) we employ and the one- and two-particle interpolators that belong to them. **K** denotes the integer-valued total momentum vector (used for the one-particle interpolator) and the arguments of the pseudoscalar interpolators are $\mathbf{k}_j = \mathbf{p}_j L/(2\pi)$.

$\pi\pi$					
N_s	**K**	(Little) group	Irrep	$\mathcal{O}_{\pi\pi}$	$\mathcal{O}_\rho$
48	(0,0,0)	O_h	T_1	$\pi(1,0,0)\pi(-1,0,0)$	ρ_x
48	(0,0,1)	C_{4v}	E	$\pi(1,0,0)\pi(-1,0,1) - \pi(-1,0,0)\pi(1,0,1)$	ρ_x
48	(0,1,1)	C_{2v}	A_1	$\pi(1,0,0)\pi(-1,1,1) + \pi(-1,0,0)\pi(1,1,1)$	$\rho_y + \rho_z$
48	(0,1,1)	C_{2v}	B_1	$\pi(1,0,0)\pi(-1,1,1) - \pi(-1,0,0)\pi(1,1,1)$	ρ_x
64	(0,0,1)	C_{4v}	E	$\pi(1,0,0)\pi(-1,0,1) - \pi(-1,0,0)\pi(1,0,1)$	ρ_x
64	(0,1,1)	C_{2v}	A_1	$\pi(1,0,0)\pi(-1,1,1) + \pi(-1,0,0)\pi(1,1,1)$	$\rho_y + \rho_z$
64	(0,1,1)	C_{2v}	B_1	$\pi(1,0,0)\pi(-1,1,1) - \pi(-1,0,0)\pi(1,1,1)$	ρ_x
$K\pi$					
N_s	**K**	(Little) group	Irrep	$\mathcal{O}_{K\pi}$	$\mathcal{O}_{K^*}$
48	(1,1,0)	C_{2v}	B_2	$\pi(1,0,0)K(0,1,0)$	$K^*_x - K^*_y$
64	(0,0,0)	O_h	T_1	$\pi(1,0,0)K(-1,0,0)$	K^*_x
64	(0,0,1)	C_{4v}	E	$\pi(1,0,0)K(-1,0,1) - \pi(-1,0,0)K(1,0,1)$	K^*_x
64	(0,1,1)	C_{2v}	A_1	$\pi(1,0,0)K(-1,1,1) + \pi(-1,0,0)K(1,1,1)$	$K^*_y + K^*_z$
64	(0,1,1)	C_{2v}	B_1	$\pi(1,0,0)K(-1,1,1) - \pi(-1,0,0)K(1,1,1)$	K^*_x

denotes an integer-valued lattice momentum vector. The choice of momenta and representations is based on the requirement that the noninteracting two-particle states lie within or close to the expected resonance widths. To allow for the reuse of the generated propagators, we restrict ourselves to $\mathbf{k}_1 = \mathbf{p}_1 L/(2\pi) = (1,0,0)$. For each total momentum **P**, we have to construct interpolators which transform according to a definite irreducible representation (irrep) of the little group of allowed cubic rotations once a Lorentz boost has been applied. We construct the interpolators using the information about the little groups given in Ref. [10]. The irreps we work with and the (one- and two-particle) interpolators that transform according to each representation are also listed in Table II. We use Schoenflies notation (see, for example, Ref. [42]) for the names of the groups and irreps.

The necessary quark-line contractions are depicted in Fig. 1, where the first row includes two-particle to two-particle transitions and the second row one- to one- as well as two- to one-meson transitions. We use stochastic $\mathbb{Z}_2 + i\mathbb{Z}_2$ wall sources at one time slice for each spin component and, for the contractions involving the two-particle interpolators, sequential inversions to generate all the contributing diagrams, following Refs. [11,14]. To compute the top left contraction of Fig. 1, it is necessary to use two stochastic sources per configuration. We use this minimum number of estimates per configuration as the gauge noise dominates. We further reduce the computational cost by fixing $\mathbf{k}_1$ to (1,0,0). Even with this restriction, we can obtain several interesting levels around the expected positions of the ρ and K^* resonances. Moreover, we only compute the full $\pi\pi \to \pi\pi$ correlator from $t = 6a$ to $t = 17a$, where we anticipate that on the one hand the signal is only moderately polluted by excited-state contributions and on the other hand statistical errors are still tolerable. We are also able to "recycle" many propagators in both $\pi\pi$ and $K\pi$ scattering.

Adding this up, in our implementation the total number of solves required on each configuration is

$$N_{\rm vec}[N_{\rm smear} + N_{p_1}(1 + 18N_{p_2} + 3N_{\rm times})], \qquad (7)$$

where $N_{\rm vec} = 8$ is the number of noise sources used (four spin components times two different vectors), $N_{\rm smear} = 4$ is the number of one-particle smearing levels (three plus one derivative source; see above), $N_{p_1} = 1$ and N_{p_2} (see Table II) are the numbers of momenta calculated and $N_{\rm times} = 12$ ($t = 6a$ up to $t = 17a$) is the number of time slices for which the box diagrams shown in the top middle and top right of Fig. 1 are calculated. For the $N_s = 48$ and $N_s = 64$ lattices, evaluating the full 8×8 matrices of correlators for each moving frame amounts to inverting the strange quark Wilson matrix 80 and 120 times, respectively, and the light quark matrix 824 and 808 times. Note that the number of solves required to compute a "traditional" point-to-all propagator is 12, i.e. the present scattering computation is by a factor of about 40 more expensive than a conventional determination of the spectrum of stable light hadrons for one quark smearing level (12 strange and 12 light quark inversions on each volume).

The momenta injected are not indicated in Fig. 1 and the correlator is the sum of all allowed momentum projections; some irreps require a combination of two related pairs of momenta and, in $\pi\pi$ scattering, we can interchange the momenta $\mathbf{p}_1$ and $\mathbf{p}_2$ carried by each pion at the sink. Similarly, we ensure that the one-particle to one-particle

correlators—depicted in the lower left of the figure—transform according to the irreps given in Table II, by taking the corresponding combinations of vector-meson polarizations. The contractions for $\pi\pi \to \rho$ and $\rho \to \pi\pi$ are complex conjugates and it is computationally cheaper to only calculate one of them. (We do this for $\pi\pi \to \rho$.) For the remaining correlation matrix elements with $i \neq j$ (one- to one-particle), we average over C_{ij} and C^*_{ji}.

C. Extraction of energy levels and phase shifts

For each kinematic situation, we construct an eight times eight matrix of correlators for our basis of interpolators in the way described above. The element of this matrix for a source interpolator $\mathcal{O}_j$ and a sink interpolator $\mathcal{O}_i$ is given as

$$C_{ij}(t) = \langle 0|\hat{\mathcal{O}}_i(t)\hat{\mathcal{O}}^\dagger_j(0)|0\rangle. \tag{8}$$

The spectral decomposition can be written as

$$C_{ij}(t) = \sum_\alpha \frac{Z^i_\alpha Z^{j*}_\alpha}{2E^\alpha} e^{-E^\alpha t}, \tag{9}$$

where $Z^i_\alpha = \langle 0|\hat{\mathcal{O}}_i|\alpha\rangle$ is the overlap factor of the state created by the operator $\hat{\mathcal{O}}^\dagger_i$ with the physical state $|\alpha\rangle$ of energy E^α. We extract the energy levels E^α by solving the generalized eigenvalue problem [43–45]

$$C(t)u^\alpha(t) = \lambda^\alpha(t_0, t)C(t_0)u^\alpha(t), \tag{10}$$

where the energy levels can be obtained from the dependence $\lambda^\alpha(t_0, t) \sim e^{-E^\alpha(t-t_0)}$ at large times.

The energies we extract are in the lab frame, so we denote these as E_L. The phase shift, however, is extracted in the center-of-momentum frame, i.e. in the rest frame of the $\pi\pi$ or πK system. It is straightforward to convert the lab-frame energies E_L into the corresponding center-of-momentum frame energies $E_{\rm cm}$.

The lab-frame energy of the two-meson state is given as

$$E_L = \sqrt{\mathbf{p}_1^2 + m_1^2} + \sqrt{\mathbf{p}_2^2 + m_2^2}, \tag{11}$$

where the m_i are the pion (or kaon) masses and the $\mathbf{p}_i$ are their momenta. In the absence of interactions the $\mathbf{p}_i^2$ are integer multiples of $(2\pi/L)^2$. The invariant squared energy in the center-of-momentum frame is

$$E^2_{\rm cm} = E_L^2 - \mathbf{P}^2, \tag{12}$$

where $\mathbf{P}$ is the total momentum of the $\pi\pi$ (or the $K\pi$) system. The square of the momentum of each of the pseudoscalars in the center-of-momentum frame is given by

$$p^2_{\rm cm} = \frac{(E^2_{\rm cm} - (m_1 + m_2)^2)(E^2_{\rm cm} - (m_1 - m_2)^2)}{4E^2_{\rm cm}}. \tag{13}$$

The phase shift is extracted, comparing the center-of-momentum-frame spectrum to the energy levels allowed by the residual cubic symmetry (little group) that corresponds to the boost applied. For each irrep, this involves an expression in terms of generalized zeta functions, derived in Refs. [9,10]. For the numerical calculation of these functions, we use the representation given in Ref. [10].

The generalized zeta function is a function of the real-valued variable $q = p_{\rm cm}L/(2\pi)$:

$$Z_{\ell m}(q^2) = \sum_{\mathbf{z}} \frac{\mathcal{Y}_{\ell m}(\mathbf{z})}{\mathbf{z}^2 - q^2}, \tag{14}$$

where $\mathcal{Y}_{\ell m}(\mathbf{z}) = |\mathbf{z}|^\ell Y_{\ell m}(\mathbf{e}_z)$ with $\mathbf{e}_z = \mathbf{z}/|\mathbf{z}|$ and $Y_{\ell m}$ are the usual spherical harmonics. The sum is over $\mathbf{z}$, the allowed momentum vectors in the boosted frame; see, e.g., Ref. [10].

For each irrep we have to consider mixing between different continuum partial waves. The relevant determinants from which the phase shifts can be extracted are listed in Ref. [10]. Here, we neglect possible mixing with partial waves $\ell \neq 1$. The s wave can only contribute to $K\pi$ scattering. Moreover, mixing of $\ell = 0$ into $\ell = 1$ is only allowed for the $\mathbf{K} = (0, 1, 1)$ A_1 irrep. We will address this case in Sec. III C below. Since the $\pi\pi$ and $K\pi$ interactions have a finite range, contributions of higher partial waves are suppressed. The $\ell = 3$ $\pi\pi$ phase shift was determined recently by Wilson and collaborators [18] at $m_\pi \approx 236$ MeV who indeed found $\delta_3 \approx 0$ near the resonance, within small errors. We conclude that limiting ourselves to $\ell \leq 1$ appears reasonable.

Subsequently, we parametrize the phase shift as a function of the center-of-momentum-frame energy using a Breit-Wigner (BW) ansatz:

$$\tan\delta = \frac{g^2}{6\pi} \frac{p^3_{\rm cm}}{E_{\rm cm}(m_R^2 - E^2_{\rm cm})}. \tag{15}$$

From this parametrization,[1] we can extract the mass of the resonance m_R and its width can be found from the coupling g as

$$\Gamma = \frac{g^2}{6\pi} \frac{p_R^3}{m_R^2}, \tag{16}$$

where p_R is the momentum carried by each particle in the center-of-momentum frame at $\delta = \pi/2$, i.e. p_R is given by $p_{\rm cm}$ of Eq. (13) for $E_{\rm cm} = m_R$.

[1]We consider alternative parametrizations in Sec. III C.

III. RESULTS

A. Determination of the energy levels

Following the generalized eigenvalue procedure detailed in Sec. II C above, we separately analyze the 8×8 matrices that cross-correlate states created by one- and two-particle interpolators for the seven $\pi\pi$ and five $K\pi$ channels listed in Table II, and obtain the respective ground and first excited-state energies. We are able to resolve these energies most easily using submatrices of correlators containing only three interpolators—one of which is always the two-particle interpolator $\mathcal{O}_{\pi\pi}$ or $\mathcal{O}_{K\pi}$ of Table II. The single-particle interpolators used in the final analysis are only of the type $\bar{\psi}\gamma_j\psi$. However, we have checked these results against employing other submatrices and found consistency of the effective masses, but no improvement. The results turned out very similar but often noisier when replacing one $\bar{\psi}\gamma_j\psi$ interpolator by $\bar{\psi}\gamma_j\gamma_t\psi$ while the $\bar{\psi}\nabla_j\psi$ interpolator increased the statistical errors very significantly, in particular for states with total momentum $\mathbf{K} = (0,1,1)$.

To save computer time we only evaluated the box diagrams in the top middle and top right of Fig. 1 for $17a \geq t \geq 6a$. The top left diagram contains two traces and naively increases like L^6 while the quark-line connected box diagrams have magnitudes $\propto L^3$. Due to this relative suppression, these can only become important at times of at least a similar magnitude as the inverse energy gap between $I = 2$ and $I = 1$ $\pi\pi$ (or $I = 3/2$ and $I = 1/2$ $K\pi$) states and probably their contribution to the $\pi\pi \to \pi\pi$ and $K\pi \to K\pi$ entries can be neglected at $t < 6a$. Nevertheless, to be on the safe side, in our generalized eigenvector analysis we set $t_0 = 6a \approx 0.43$ fm.

We show effective masses

$$E^{\alpha}_{L,\mathrm{eff}}(t + a/2) = \frac{1}{a}\ln\frac{\lambda^{\alpha}(t_0 = 6a, t)}{\lambda^{\alpha}(t_0 = 6a, t + a)} \qquad (17)$$

for some of our $\pi\pi$ and $K\pi$ eigenvalues [see Eq. (10)], in Fig. 2, for the region $t > t_0 + a$. To enable better comparison to other studies, we display the data in physical units. The effective masses are typically consistent with plateaus between $t = 10a \approx 0.71$ fm and $17a \approx 1.22$ fm, which is our most frequent fit range, although there are differences between the channels. The $K\pi T_1$ channel shown in the figure is an extreme example, where the fit range starts at $t = 14a \approx 1$ fm.

Of particular interest are the $\mathbf{K} = (0,1,1)$ A_1 channels. The noninteracting ground states in this irrep correspond to a momentum distribution $\mathbf{k}_1 = \mathbf{0}$ and $\mathbf{k}_2 = \mathbf{K} = (0,1,1)$ among the two pseudoscalar mesons that differs from the one used in constructing our two-particle interpolators ($\mathbf{k}_1 = (1,0,0)$ and $\mathbf{k}_2 = \mathbf{K} - \mathbf{k}_1 = (-1,1,1)$). In principle, these correlation functions could decay towards the lower-lying states. However, we find no indication for this in our data (see Fig. 2), and conclude that our interpolators effectively decouple from these energy levels.

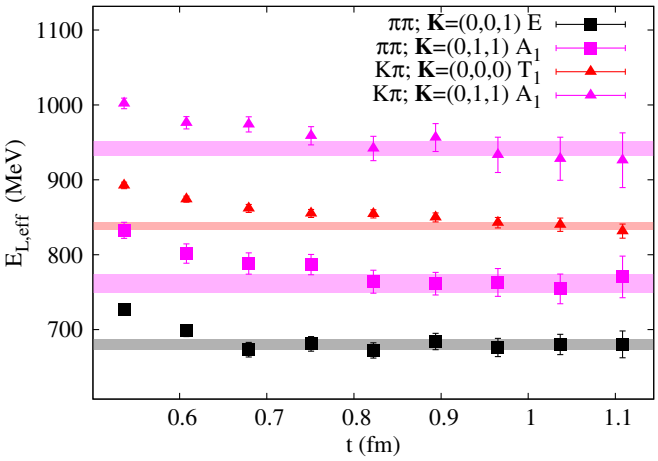

FIG. 2. Effective masses for some $\pi\pi$ and $K\pi$ channels. The error bands correspond to the fit results.

The resulting lab-frame energy levels E_L are shown in Fig. 3 both for the $\pi\pi$ and $K\pi$ channels. The scale is set using $a^{-1} = 2.76$ GeV, ignoring the 3% overall scale uncertainty for the time being. The statistical errors are obtained using the jackknife procedure. Only two $\pi\pi$ levels are above the four-pion threshold [the excited states in the

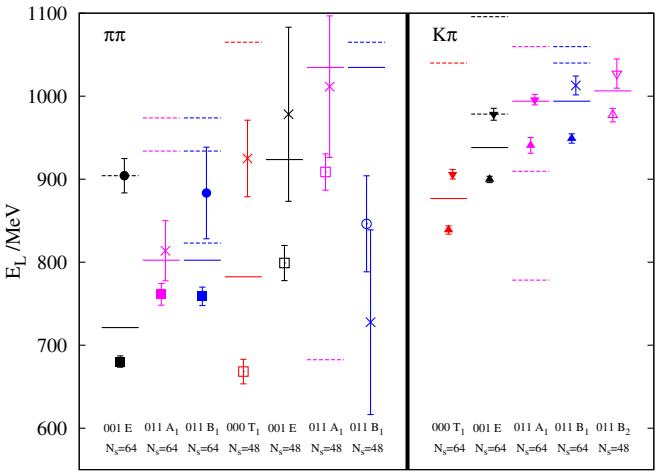

FIG. 3. Energy levels of the $\rho|\pi\pi$ (left) and $K^*|K\pi$ (right) systems in finite boxes of linear sizes $N_s a = 48a \approx 2.6/m_\pi^\infty \approx 3.4$ fm and $N_s a = 64a \approx 3.5/m_\pi^\infty \approx 4.6$ fm for different lattice momenta and representations in the laboratory frame. Horizontal lines correspond to the energy levels of a noninteracting two-particle system. Squares and upward-pointing triangles indicate ground states, while circles and downward-pointing triangles indicate first excited states. Open symbols correspond to the smaller volume and full symbols to the larger volume. Crosses are for levels that are not used in our subsequent phase-shift analysis. Note that for $\pi\pi$ scattering the excited states in both $\mathbf{K} = (0,0,1)$ E channels are above the respective noninteracting 4π thresholds (not shown).

$\mathbf{K} = (0,0,1)$ E irrep], one of which will be disregarded in any case in the phase-shift analysis below.

In the figure, we also show the energies of the noninteracting two-particle states. The solid horizontal lines are the noninteracting levels corresponding to the two-particle interpolators explicitly included in our basis (given in Table II), while the dashed lines correspond to other distributions of the momentum among the noninteracting pseudoscalar mesons. As we have not included interpolators that explicitly resemble these momentum configurations, we cannot rely on our extracted energy levels to be sensitive to their presence and ignore these noninteracting levels in our phase-shift analysis. As already discussed above, in the A_1 case the noninteracting ground states are lower in energy than the levels that correspond to the momentum distribution we have implemented (solid lines). Nevertheless, we see no evidence of any coupling of the interpolators within our basis to these states; see Fig. 2. Note that for the $N_s = 64$ $\pi\pi$ channel this level lies at 561 MeV, below the energy region shown in Fig. 3.

Levels that are irrelevant, due to large statistical errors for the resulting phase shifts, will be excluded from our subsequent analysis. These levels are depicted as crosses in Fig. 3. We remind the reader that the deviations of the measured energy levels shown in the figure from the noninteracting two-particle levels (solid lines) are due to the ρ and K^* resonances and encode the resonance parameters.

B. Phase shift and resonance parameters

The center-of-momentum-frame energies $E_{\rm cm}$ and phase shifts $\delta(E_{\rm cm})$ can both be extracted from measured lab-frame energy levels E_L in a given irrep (see Sec. II C), where we assume $m_\pi = 149.5$ MeV, in spite of the fact that the measured pion mass on the small volume is larger by 10 MeV. This will be addressed in Sec. III C below.

We plot $\delta(E_{\rm cm})$ in Fig. 4, using the same color and symbol scheme as in Fig. 3. As explained above, in our determination of the phase shift we assume that one value of ℓ ($\ell = 1$) dominates, such that there is a one-to-one correspondence between the extracted energy levels and the points in the phase-shift curves. For clarity we omit all data points from the figure with errors on the phase shift in excess of $\pi/5$ (marked as crosses in Fig. 3). These have little statistical impact and will therefore be excluded from our analysis.

The $\pi\pi$ and $K\pi$ phase shifts are each fitted to the BW resonance form given in Eq. (15). Our fit to the $\pi\pi$ phase shift results in $\chi^2/\text{d.o.f} = 8.9/7$ and for the $K\pi$ phase shift we obtain $\chi^2/\text{d.o.f} = 19.2/7$. These fits are included in Fig. 4 (the grey hashed band for $\pi\pi$ scattering and the solid orange one for $K\pi$ scattering). In the $\pi\pi$ case the dashed data point of the figure is slightly above the respective 4π threshold. However, as discussed in the Introduction, the effect of this inelastic threshold is expected to be negligible.

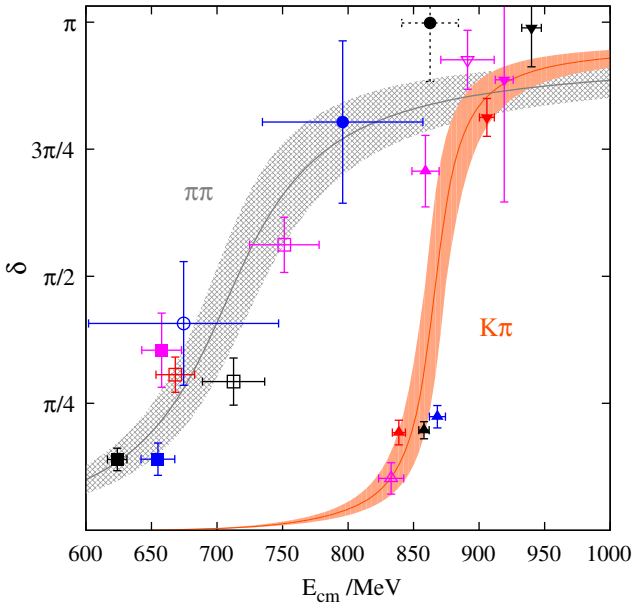

FIG. 4. The phase shift as a function of the center-of-momentum-frame energy, $E_{\rm cm}$, for p-wave $\pi\pi$ scattering around the ρ resonance and $K\pi$ scattering around the K^* resonance. The data correspond to the lab-frame energies shown in Fig. 3, with matched colors and symbols. The curves with error bands are Breit-Wigner parametrizations. The dashed error bar indicates a point in $\pi\pi$ scattering which lies above the four-pion threshold.

Moreover, excluding this point from the fit only produces a hardly visible change. Since we have exact isospin symmetry in place, decays into three-pion final states are not possible.

Figures 3 and 4 clearly show an increase in statistical noise when going to smaller quark masses: the $\pi\pi$ scattering data have considerably larger error bars than the $K\pi$ data. From the BW fits shown, we find the values

$$m_\rho = 716(21)(21)\ \text{MeV}, \qquad m_{K^*} = 868(8)(26)\ \text{MeV}, \tag{18}$$

$$g_{\rho\pi\pi} = 5.64 \pm 0.87, \qquad g_{K^*K\pi} = 4.79 \pm 0.49, \tag{19}$$

$$\Gamma_\rho = 113(35)(3)\ \text{MeV}, \qquad \Gamma_{K^*} = 30(6)(1)\ \text{MeV}, \tag{20}$$

for $\pi\pi$ and $K\pi$ scattering, where the first errors are statistical and the second errors reflect our 3% overall scale uncertainty [31]. In the last row we also quote the corresponding decay widths, obtained via Eq. (16). From a given parametrization of the p-wave phase shift, assuming partial wave unitarity and ignoring further inelastic thresholds, we can analytically continue to the second (unphysical) Riemann sheet (see, e.g., Ref. [46]) and determine the position of the resonance pole. Using the BW parametrization, for the ρ and K^* resonances we find $\sqrt{s_R} = [707(17) - \text{i}55(18)]$ MeV and $\sqrt{s_R} = [868(10) - \text{i}14.4(3.4)]$ MeV, respectively. These numbers are

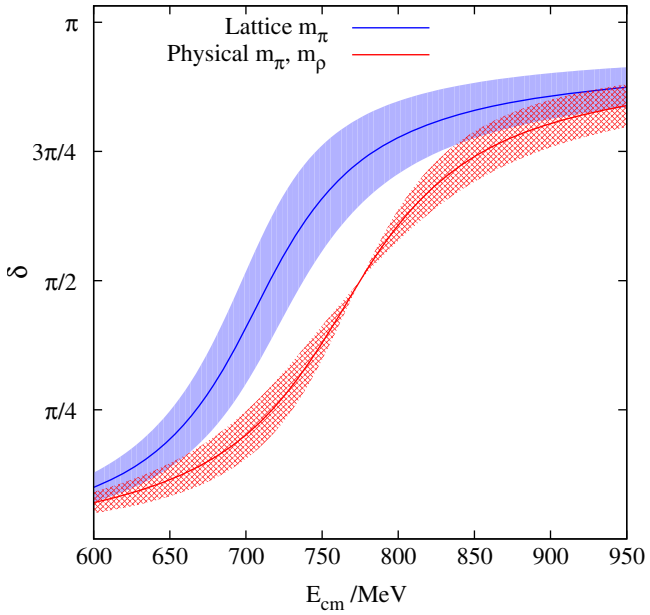

FIG. 5. We compare phase-shift curves for $\pi\pi$ scattering around the ρ resonance for our fitted Breit-Wigner resonance (solid blue band) and one with the fitted coupling but physical pion and ρ masses (hashed red band).

consistent with $\sqrt{s_R} = m_R - \mathrm{i}\Gamma/2$ from the BW fits (18) and (20). Note, however, that $\mathrm{Re}\sqrt{s_\rho}$ is by about half a standard deviation smaller than the BW fit parameter m_ρ. In Sec. III C we will explore in detail the parametrization dependence of these results.

We emphasize that our study was carried out at a single lattice spacing only, which is not reflected in the errors given above. Both resonant masses come out smaller than the experimental values, 775 and 896 MeV, respectively. The reduced decay phase space, due to a 10% heavier-than-physical pion, in conjunction with somewhat smaller-than-physical resonance masses, is the main reason why our decay widths appear to be somewhat below the experimental ones, $\Gamma_\rho \approx 148$ MeV and $\Gamma_{K^*} \approx 47$ MeV, although this difference is only statistically significant for the K^*. The coupling $g_{\rho\pi\pi}$ is consistent with the experimental value $g_{\rho\pi\pi} \approx 5.93$ while our $g_{K^*K\pi}$ is slightly lower than $g_{K^*K\pi} \approx 5.39$. The ordering $g_{\rho\pi\pi} > g_{K^*K\pi}$ is reproduced, albeit within large errors.

In Fig. 5 the $\pi\pi$ phase-shift curve fitted to our data is compared to the same curve with the π and ρ masses set to their physical values [25], but with the coupling $g_{\rho\pi\pi}$ taken from our fit (19). The latter curve is forced to run through $\delta = \pi/2$ at the fixed resonant mass $E_R = E_{\mathrm{cm}} = 775$ MeV as we use the BW parametrization. Since our value of $g_{\rho\pi\pi}$ agrees with experiment, experimental data will be described by the hashed red band. Again, there is an overall scale-setting uncertainty of 3% on E_{cm}, corresponding to 20 MeV, that we do not display as well as other systematics, most notably a 10% heavier-than-physical pion and a fixed lattice spacing. The figure illustrates that also in terms of the width of the resonance we are close to the physical case. Previous studies of $\pi\pi$ scattering have not directly addressed the physical limit, although unitarized chiral perturbation theory has been used in Ref. [47] to extrapolate lattice data obtained at $m_\pi \approx 236$ MeV [18] to the physical point.

C. Investigation of possible biases

Here we investigate the effects on the extracted resonance parameters, of the finite-volume pion mass shift, of the BW parametrization we use to fit $\delta(E_{\mathrm{cm}})$ and of the presence of inelastic thresholds. We also address the possibility of an $\ell = 0$ pollution for the case of $K\pi$ scattering.

The pion mass enters the generalized zeta function, Eq. (14), via the calculation of the momentum carried by the two particles in the center-of-momentum frame, given by Eq. (13). We prefer to use the infinite-volume pion and kaon masses throughout because we are relating the spectra to scattering amplitudes in an infinite volume. For the larger $L = 64a$ lattice size, the pion mass determined in the finite volume and that extrapolated to infinite volume differ by as little as 0.2 MeV [32]. However, the pion mass measured on the $L = 48a$ configurations differs from the infinite-volume mass by 10 MeV and the kaon mass by 3 MeV. Since pion exchanges around the boundaries of the periodic box go beyond the Lüscher formalism, we have repeated the analysis using finite-volume pion masses instead, to explore these systematics. For the $L = 64a$ data the effect obviously is insignificant. For $L = 48a$ the phase shifts for the corresponding six points (four for the ρ resonance and two for K^*) depicted in Fig. 4 (open symbols) increase by values ranging from 0.03 to 0.05. These differences are considerably smaller than our errors on δ. Indeed, using these numbers instead, we find the ρ and K^* resonance parameters $m_\rho = 713(18)$ MeV, $m_{K^*} = 867(7)$ MeV, $g_{\rho\pi\pi} = 5.56(85)$ and $g_{K^*K\pi} = 4.81(51)$, in almost perfect agreement with our main analysis employing the infinite-volume pion mass (18) and (19). For instance, the central values for the masses deviate by only -3 and -1 MeV, respectively. Adding these systematics to the statistical errors in quadrature has no impact.

Next, we replace the BW parametrization of the scattering phase shift [see Eq. (15)], by other functional forms suggested in Ref. [16] and references therein. We write,

$$\tan\delta = \frac{E_{\mathrm{cm}}\Gamma(E_{\mathrm{cm}})}{m_R^2 - E_{\mathrm{cm}}^2}, \qquad \Gamma^{(0)}(E_{\mathrm{cm}}) = \frac{g^2}{6\pi}\frac{p_{\mathrm{cm}}^3}{E_{\mathrm{cm}}^2}, \qquad (21)$$

TABLE III. ρ resonance: Fit results for various phase-shift models. The square root of the resonance pole position s_R may be used to define $\sqrt{s_R} = m_R - \frac{i}{2}\Gamma_R$. The errors given are statistical only.

Model	m_ρ/MeV	$g_{\rho\pi\pi}$	other fit parameters	$\sqrt{s_R}$/MeV
0: Eq. (15) (BW)	716(21)	5.64(87)	⋯	$707(17) - \frac{i}{2}110(36)$
1: Eq. (22)	717(23)	5.38(84)	$R = 3(6)$ GeV^{-1}	$714(26) - \frac{i}{2}104(35)$
2: Eq. (23)	718(23)	5.34(84)	$\beta = 0.16(15)$ GeV	$716(29) - \frac{i}{2}103(35)$
3: Eq. (24)	717(23)	⋯	$B_0 = 1.31(45)$, $B_1 = 1.6(3.0)$	$714(26) - \frac{i}{2}103(37)$

where $\Gamma = \Gamma(m_R)$ is the resonance width and the energy-dependent width function $\Gamma(E_{\rm cm})$ equals $\Gamma^{(0)}(E_{\rm cm})$ in the BW case. In addition, we use [48–50][2]

$$\Gamma^{(1)}(E_{\rm cm}) = \frac{g^2}{6\pi}\frac{p_{\rm cm}^3}{E_{\rm cm}^2}\frac{1+(p_R R)^2}{1+(p_{\rm cm}R)^2}, \tag{22}$$

$$\Gamma^{(2)}(E_{\rm cm}) = \frac{g^2}{6\pi}\frac{p_{\rm cm}^3}{E_{\rm cm}^2}\exp\left(\frac{p_R^2 - p_{\rm cm}^2}{6\beta^2}\right), \tag{23}$$

$$\Gamma^{(3)}(E_{\rm cm}) = 2\frac{p_{\rm cm}^3}{E_{\rm cm}^2} \times \left(B_0 + B_1\frac{E_{\rm cm} - \sqrt{s_0 - E_{\rm cm}^2}}{E_{\rm cm} + \sqrt{s_0 - E_{\rm cm}^2}}\right)^{-1}, \tag{24}$$

where $s_0 = (2m_\pi + m_R)^2$. The BW fit function depends on two fit parameters, the resonant mass m_R and the coupling g, while the other parametrizations depend on three parameters: $\Gamma^{(1)}$ contains the additional parameter R, $\Gamma^{(2)}$ contains $\beta \sim 1/(\sqrt{6}R)$ and g is replaced by B_0 and B_1 within $\Gamma^{(3)}$.

Our fit results for $\pi\pi$ scattering are shown in Table III. In all cases the additional parameter (R, β and B_1) turned out to be consistent with zero. All the resonant masses we obtain are in perfect agreement with the BW result shown in the first row. Also the widths are compatible with the BW width $\Gamma^{(0)} = 113(35)$ MeV of Eq. (20) and the parameter $B_0 = 1.31(45)$ is consistent with the expectation $B_0 \approx 1.07$, extracted from experimental data in Ref. [50]. Interestingly, we observe the numerically biggest difference (half a standard deviation) between the energy at a phase shift $\delta = \pi/2, m_\rho = E_{\rm cm}(\pi/2)$, and the real part of $\sqrt{s_R}$ for the BW parametrization. We conclude from Table III that within our precision, we can neither differentiate between the different models nor distinguish the pole position in the second Riemann sheet from the naively fitted mass and width.

In our determination of the $\pi\pi$ energy levels, we noted that there was one data point above the four-pion threshold (the dashed point of Fig. 4). Excluding this from any of our four fits, however, had no impact worthy of mentioning.

For $K\pi$ scattering, in the case of the $\mathbf{K} = (0,1,1)$ A_1 irrep, we cannot exclude the possibility of a $\ell = 0$ partial wave admixture. Therefore, we perform all fits [setting $s_0 = (m_\pi + m_K + m_R)^2$ in Eq. (24)] including and excluding the corresponding two data points; see the pink solid triangles in Figs. 3 and 4. The resulting fit parameters and the position of the K^* pole are displayed in Table IV. When including the two A_1 points, there is no sensitivity to the additional fit parameters and all the results are remarkably stable. Including and excluding these points, real and 2i times the imaginary part of $\sqrt{s_R}$ perfectly agree with the fitted masses and widths obtained through Eqs. (21)–(24), as one would expect for $\Gamma_{K^*}/m_{K^*} \approx 0.035 \ll 1$. Removing the two points, however, appears to increase the resonant mass. Also the fit results become less stable since the BW fit has only five remaining degrees of freedom while the other three fits have only four.

In conclusion, while we find $g_{K^*K\pi}$ to be very stable against variations of the parametrization and of the number of points fitted, the K^* mass is somewhat affected by the latter. Therefore, we allow for another systematic error of 10 MeV to be added to the statistical error shown in Eq. (18) in quadrature:

$$m_{K^*} = 868(13)(26)\ \text{MeV}. \tag{25}$$

D. Investigation of an alternative method

It is possible to estimate the value of the coupling $g_{\rho\pi\pi}$ directly from the correlators, using the McNeile-Michael-Pennanen (MMP) method introduced in Refs. [51,52] (also see Refs. [53,54] for earlier, related work), if the momentum and volume are selected such that the $\pi\pi$ energy is close to the resonant mass $m_\rho = m_R$. This method was also employed recently for studying the Δ resonance [55].

Using the correlators defined in Eq. (8), with $\mathcal{O}_1$ and $\mathcal{O}_2$ being two- and one-particle interpolators, we can extract (approximate) ground-state energies $E_{\pi\pi}$ and E_ρ from $C_{11}(t)$ and $C_{22}(t)$ alone, respectively, at times sufficiently small to avoid the higher level decaying into the lower level (if $E_\rho \neq E_{\pi\pi}$) and large enough for excited-state contributions to be negligible. In this situation, the ground-state contribution to $C_{12}(t)$ reads

$$C_{12}(t) \approx xa\sum_{t'}\frac{Z_{\pi\pi}^1 Z_\rho^{2*}}{2\sqrt{E_{\pi\pi}E_\rho}}e^{-E_{\pi\pi}(t-t')}e^{-E_\rho t'}, \tag{26}$$

[2]Note that B_0 is defined differently in Ref. [16] than here [50].

TABLE IV. K^* resonance: Fit results for various phase-shift models, including and excluding the two $\mathbf{K} = (0,1,1)$ A_1 irrep points that may also couple to the $\ell = 0$ partial wave. The errors given are statistical only.

Model	A_1 included	m_{K^*}/MeV	$g_{K^*K\pi}$	other fit parameters	$\sqrt{s_R}$/MeV
0: Eq. (15) (BW)	yes	868(8)	4.79(49)	⋯	$866(7) - \frac{\mathrm{i}}{2}30(7)$
1: Eq. (22)	yes	868(9)	4.78(44)	$R = 6(29)$ GeV^{-1}	$868(9) - \frac{\mathrm{i}}{2}30(7)$
2: Eq. (23)	yes	868(9)	4.80(47)	$\beta = 0.13(45)$ GeV	$867(10) - \frac{\mathrm{i}}{2}30(8)$
3: Eq. (24)	yes	868(9)	⋯	$B_0 = 3.2(5.3)$, $B_1 = 8.2(28.9)$	$868(10) - \frac{\mathrm{i}}{2}29(7)$
0: Eq. (15) (BW)	no	873(9)	5.08(43)	⋯	$871(8) - \frac{\mathrm{i}}{2}35(7)$
1: Eq. (22)	no	878(10)	5.09(38)	$R = 1.2(1.6)$ MeV^{-1}	$877(10) - \frac{\mathrm{i}}{2}36(6)$
2: Eq. (23)	no	887(7)	4.42(69)	$\beta = 58(13)$ MeV	$890(7) - \frac{\mathrm{i}}{2}27(9)$
3: Eq. (24)	no	886(8)	⋯	$B_0 = 10(5)$, $B_1 = 44(25)$	$888(9) - \frac{\mathrm{i}}{2}24(6)$

where Z_α^i are the amplitudes to create the states $|\alpha\rangle$ using $\hat{\mathcal{O}}_i^\dagger$. These overlap factors also appear within $C_{11}(t)$ and $C_{22}(t)$ [see Eq. (9)] and will cancel as we are going to divide C_{12} by an appropriate combination of these two elements in Eqs. (28) and (29) below. The ρ state created at $t = 0$ will propagate to a time $t' < t$, where it undergoes a transition into $\pi\pi$. x is the associated $\rho \to \pi\pi$ transition amplitude and in Eq. (26) we summed over all possible intermediate times t'. The underlying assumption is that the overlaps of $\hat{\mathcal{O}}_2^\dagger|0\rangle$ with $|\pi\pi\rangle$ and of $\hat{\mathcal{O}}_1^\dagger|0\rangle$ with $|\rho\rangle$ are small and can be treated as perturbations, at least if t is not taken too large. Obviously, there are corrections of higher order in x to Eq. (26).

The coupling $g_{\rho\pi\pi}$ can then be estimated from x through [52]

$$g_{\rho\pi\pi}^2 \approx \frac{L^3 E_{\mathrm{cm}}^3}{4 p_{\mathrm{cm}}^2} |x|^2. \tag{27}$$

This can be seen as follows [52]. Fermi's golden rule relates the decay width to the matrix element x in the center-of-momentum frame: $\Gamma \approx |x|^2 L^3 p_{\mathrm{cm}} E_{\mathrm{cm}}/(24\pi)$. This can be reexpressed in terms of g^2 through $\Gamma = g^2 p_{\mathrm{cm}}^3/(6\pi E_{\mathrm{cm}}^2)$ [see Eq. (16)], where E_{cm} is taken at the point $\delta = \pi/2$. The prefactor $L^3 p_{\mathrm{cm}} E_{\mathrm{cm}}/(24\pi)$ above contains the following contributions: 2π from the golden rule, $L^3 p_{\mathrm{cm}} E_{\mathrm{cm}}/(8\pi^2)$ from the density of states, $1/2$ for a decay into identical pions and $1/3$, averaging over one pion momentum direction for the fixed ρ polarization and momentum.

In Eq. (27) several assumptions have been made. 1) The golden rule is applicable, i.e. the $\pi\pi$ contribution to the initial ρ meson state is insubstantial and the matrix element is not too large: $|x|t \ll 1$. This is synonymous with neglecting terms of higher order in x. 2) The volumes are sufficiently large for continuous density of states methods to be applicable. 3) The $\pi\pi$ and ρ states have a similar energy and, in the center-of-momentum frame, this is close to the resonant mass. 4) x does not change substantially when transforming it from the lab to the center-of-momentum frame.

In the limit $E_{\pi\pi} = E_\rho$, summing over the intermediate time t', the ground-state contribution to Eq. (26) has the time dependence $te^{-E_{\pi\pi}t}$, while excited states are suppressed by a power of t, relative to this. In this case, x can be found from a ratio of correlators as

$$\frac{|C_{12}(t)|}{\sqrt{C_{11}(t)C_{22}(t)}} \approx \mathrm{const} + xt, \tag{28}$$

up to exponential corrections in t that contribute at small times and neglecting higher powers of xt. Since only $|x|^2$ is relevant, above we defined x as real and positive. When the difference $\Delta E = E_{\pi\pi} - E_\rho$ is nonzero, we can still perform the sum over t' in Eq. (26). In this case the time dependence of the ground-state contribution is $a[\sinh(\Delta E t/2)/\sinh(\Delta E a/2)]e^{-\bar{E}t}$ (see, e.g., Ref. [55]), where the average energy is defined as $\bar{E} = \frac{1}{2}(E_{\pi\pi} + E_\rho)$. The ground-state contribution of the ratio of correlators can again be used to extract x:

$$R(t) \equiv \frac{|C_{12}(t)|}{\sqrt{C_{11}(t)C_{22}(t)}} \frac{t \sinh(\Delta E a/2)}{a \sinh(\Delta E t/2)} \approx \mathrm{const} + xt, \tag{29}$$

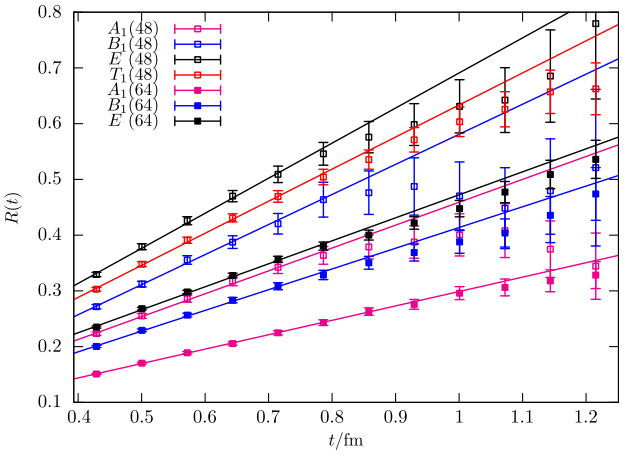

FIG. 6. The ratio of correlators $R(t)$ defined in Eq. (29) for different irreps on the two volumes (see Table V), together with linear fits to the first seven data points shown.

TABLE V. Estimates of x and $g_{\rho\pi\pi}$ using the MMP method [51,52]. The entries are sorted in terms of a descending gap $\Delta E = E_{\pi\pi} - E_\rho$. In the last row we show our result Eq. (19) from the Lüscher-type scattering analysis for comparison.

N_s	**K**	Irrep	ΔE/MeV	x/MeV	$g_{\rho\pi\pi}$
48	(0,1,1)	A_1	135	81(5)	5.54(30)
48	(0,1,1)	B_1	95	106(7)	7.07(44)
48	(0,0,1)	E	16	124(6)	8.37(39)
48	(0,0,0)	T_1	−35	113(4)	7.54(28)
64	(0,1,1)	A_1	−122	51(2)	5.19(17)
64	(0,1,1)	B_1	−140	73(3)	8.18(22)
64	(0,0,1)	E	−173	81(2)	7.46(25)
Full scattering analysis			⋯	⋯	5.64(87)

where we estimate ΔE from the exponential decay of the ratio $C_{11}(t)/C_{22}(t)$ at large (but not too large) times.

We now proceed to estimate $g_{\rho\pi\pi}$ to assess the reliability of the MMP method. In Fig. 6 we show the resulting ratios $R(t)$, together with linear fits to the first seven data points, $6a \le t \le 12a$. The color coding of the symbols corresponds to that of Fig. 3. The extracted slopes vary between 51 and 124 MeV with the smaller slopes corresponding to the larger volume (full symbols), as one would expect from the naive scaling with $L^{-3/2}$ of the amplitude x defined in Eq. (26). This scaling is also consistent with Eq. (27), where the combination x^2L^3 appears. For the largest slope $x \approx 124$ MeV and $t = 12a \approx 0.86$ fm, we obtain $xt \approx 0.54$. Indeed, around this Euclidean time higher-order corrections in xt become relevant, while for the large volume data sets, where the slopes are smaller, the linear behavior persists for much longer. We see no indication of exponential corrections towards small times.

In Table V we show the results for x and the derived couplings, where the errors are purely statistical. More details on the momenta and interpolators used can be found in Table II. The entries of Table V are ordered in terms of decreasing ΔE, where we find that a smaller ΔE corresponds to a smaller $E_{\rm cm}$ (and a smaller phase shift δ); see Fig. 4. Naively, the T_1 and E irreps on the $N_s = 48$ lattice should give the most reliable results as these are closest to the resonance and best matched in terms of a small ΔE. However, only the values from the A_1 irreps are in agreement with the result from our Lüscher-type scattering analysis. We remark that in terms of the kinematics the B_1 irrep is similar to A_1, except for the orientation of the ρ spin relative to the lattice momentum $\mathbf{K} = (0, 1, 1)$. These pairs of irreps are also close to each other in terms of their ΔE values. Nevertheless, the results from the B_1 irrep differ substantially from the expectation.

Using the Lüscher method [1] has the advantage that we can directly determine the phase shift, without relying on a BW parametrization or introducing an effective coupling $g_{\rho\pi\pi}$. Moreover, the systematics can be controlled, while the MMP method [51,52] relies on several approximations that cannot be tested easily. However, the statistical errors are smaller using the MMP method than in our full-fledged scattering analysis. In principle we did not even have to evaluate the box diagram in the upper row of Fig. 1 as formally this is of order x^2, beyond the first-order perturbative ansatz. While it is encouraging that the couplings obtained are of sizes similar to the correct result, they scatter substantially between volumes and representations. Therefore, we have to assume a systematic uncertainty of the MMP method for ρ decay on our volumes of about 50%, in terms of the coupling $g_{\rho\pi\pi}$.

E. Comparison to previous results

In Fig. 7, we compare our results on the ρ meson mass, extracted from the phase-shift position $\delta = \pi/2$ of the BW fit to various results from the literature [6,11,13–16,18–20]. These results were obtained using different methods, lattice

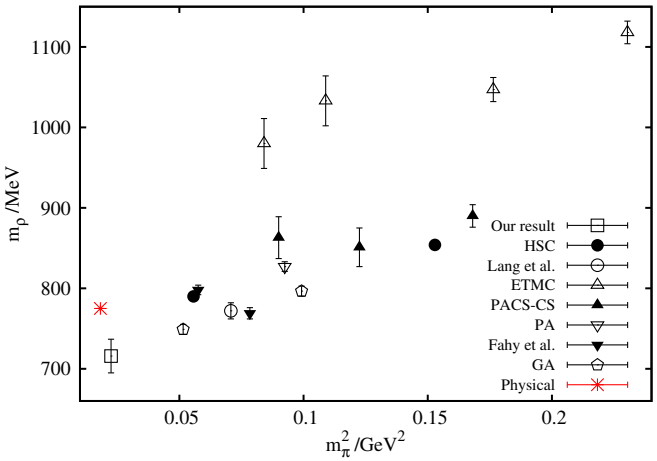

FIG. 7. ρ resonance masses from this (leftmost open square) and previous lattice calculations by the Hadron Spectrum Collaboration (HSC) [16,18], Lang *et al.* [13], ETMC [6], PACS-CS [11,14], Pelissier and Alexandru (PA) [15], Bulava *et al.* [19] and Guo and Alexandru (GA) [20]. The physical value is also plotted [25]. Open symbols correspond to simulations with $N_f = 2$ sea quark flavors, and full symbols correspond to $N_f = 2 + 1$. In none of the cases was the continuum limit taken and no study includes systematic errors.

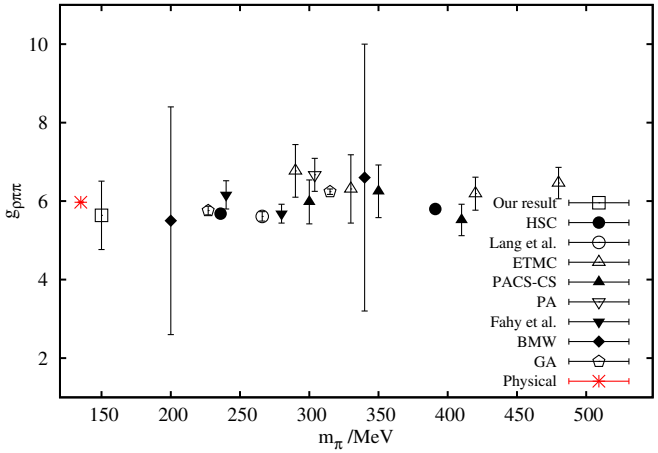

FIG. 8. Breit-Wigner couplings from various lattice calculations (Hadron Spectrum Collaboration (HSC) [16,18], Lang *et al.* [13], ETMC [6], PACS-CS [11,14], Pelissier and Alexandru (PA) [15], Bulava *et al.* [19], BMW-c [12] and Guo and Alexandru (GA) [20]) and that extracted from the experimentally measured ρ meson width [25]. Open symbols correspond to $N_f = 2$ results, and full symbols correspond to $N_f = 2 + 1$.

actions, lattice spacings and $N_f = 2$ (open symbols) as well as $N_f = 2 + 1$ (full symbols) sea quark flavors. In none of the cases was a continuum limit extrapolation attempted and we only show our statistical error as the errors of the other data do not contain systematics. In most of these cases BW masses are quoted, which is why we compare these to our BW mass. In Refs. [56,57] next-to-leading-order (NLO) and next-to-next-to-leading-order (NNLO) chiral perturbation theory, combined with the inverse amplitude method, are used to predict the pion mass dependence of m_ρ. The quality of the available lattice data does not yet allow for a detailed comparison. The general trend seen in the majority of lattice calculations qualitatively agrees with a linear dependence of m_ρ on m_π^2, as suggested by leading-order chiral perturbation theory; however, there are notable outliers.

In Fig. 8 we show the coupling $g_{\rho\pi\pi}$, obtained in Refs. [6,11–16,18–20]. Up to $m_\pi \approx 400$ MeV, Ref. [57] expected the coupling $g_{\rho\pi\pi}$ to decrease (increase) by about 5% at NLO (NNLO), as a function of the pion mass, i.e., within the accuracy of their approach, $g_{\rho\pi\pi}$ is constant and the reduction of the decay width is purely due to phase space. An almost constant behavior is also suggested by the Kawarabayashi-Suzuki-Riazuddin-Fayyazuddin relation [58,59], $g_{\rho\pi\pi} \approx m_\rho/f_\pi \approx 5.96$, where $f_\pi = \sqrt{2}F_\pi \approx 130$ MeV at the physical point. In Fig. 8, indeed, the lattice values for pion masses up to $m_\pi \approx 470$ MeV are all around this coupling (which is indistinguishable from the physical coupling $g_{\rho\pi\pi} \approx 5.93$, also shown in the figure). However, the noise increases significantly, closer to the physical pion mass, so $g_{\rho\pi\pi}$ can be extracted much more accurately at large quark masses. Again note that the lattice results were obtained at different lattice spacings with different actions and have quite different systematics.

For $K\pi$ scattering only a few previous lattice studies exist. At $m_\pi \approx 150$ MeV and at our lattice spacing, we find [Eqs. (25) and (19)] $m_{K^*} = 868(13)(26)$ MeV and $g_{K^*\pi\pi} = 4.79(49)$. Note that in experiment $m_{K^*} \approx 896$ MeV and $g_{K^*K\pi} \approx 5.39$. The Hadron Spectrum Collaboration [24] reports $m_{K^*} = 933(1)$ MeV and $g_{K^*K\pi} = 5.72(52)$ at a pion mass of 391 MeV. Prelovsek *et al.* [22] used $m_\pi = 266$ MeV and obtained $m_{K^*} = 891(14)$ MeV and $g_{K^*K\pi} = 5.7(1.6)$ while Fu and Fu [21] found $m_{K^*} = 1014(27)$ MeV and $g_{K^*\pi\pi} = 6.38(78)$, using a lattice spacing of 0.15 fm and a pion mass of 240 MeV.

IV. CONCLUSIONS

In summary, we have demonstrated the feasibility of computing resonance scattering parameters at a nearly physical pion mass. In particular, we computed the p-wave scattering phase shifts for $\pi\pi$ scattering in the $I = 1$ channel and $K\pi$ in the $I = 1/2$ channel. From these, we extracted the masses and couplings $m_\rho = 716(21)(21)$ MeV, $\Gamma_\rho = 113(35)(3)$ MeV, $m_{K^*} = 868(13)(26)$ MeV and $\Gamma_{K^*} = 30(6)(1)$ MeV. The masses are lower than the experimental ones, $m_\rho \approx 775$ MeV, $m_{K^*} \approx 896$ MeV, and at least the width of the K^* meson is underestimated too, in part due to a 10% heavier-than-physical pion. The values from experiment are $\Gamma_\rho \approx 148$ MeV, $\Gamma_{K^*} \approx 47$ MeV [25]. The second errors reflect an overall scale uncertainty of 3% [31]. While for the ρ meson mass and width this error can be added in quadrature to the statistical one, for the K^* parameters it is not straightforward to account for this uncertainty as our strange quark mass was tuned, assuming $a^{-1} = 2.76$ GeV. It is clear that we undershot the experimental ρ resonance mass by about two standard deviations, which indicates that not all systematics have been accounted for; in particular only one (albeit small) lattice spacing was realized. The corresponding positions of the resonance poles in the second Riemann sheet from analytical continuation are shown in Tables III and IV and, at our present level of error, these cannot be distinguished from the above Breit-Wigner fit results.

The stochastic one-end source method we have used is cheaper compared to other methods [17,60,61], as long as the set of kinematic points (and interpolators) is suitably restricted. In our calculation, we were able to recycle many propagators, by keeping one of the momenta, $\mathbf{p}_1$, fixed. The number of inversions required is given in Eq. (7) and the cost of including additional momenta is large. This is a limitation in particular for larger volumes, when the density of states increases and the use of multiple two-particle interpolators cannot be avoided. We remark, however, that our larger volume with a linear lattice extent $64a \approx 4.6$ fm is not at all

small considering present-day standards in lattice scattering computations.

An alternative approach is the distillation method [60], which has been used in several other scattering calculations [13,16,18]. This method does not suffer from a large computational overhead when including additional momenta as time-slice-to-all propagators (perambulators) are used in constructing the correlators. However, this method is not very well suited to large volumes as the number of vectors required increases in proportion to L^3N_t and the cost of contractions also scales with a power of the number of vectors. Combining this method with stochastic estimates [61] may ultimately not change this scaling behavior but may make realistic lattice sizes accessible. Indeed, this stochastic distillation method has been successfully employed for $\pi\pi$ scattering [17,19], where the number of solves used in Ref. [19] is not much higher than ours. It will be very interesting to see if such calculations can be pushed towards small quark masses, large volumes and time distances of about 1 fm that allow for a reliable extraction of energy levels. Stochastic distillation was also successfully used to study DK scattering [62–64].

Our calculation is performed at a single lattice spacing and it is not possible to quantify the size of discretization effects. For the action we use, these are of $\mathcal{O}(a^2)$ and it is unlikely at our lattice spacing $a \approx 0.071$ fm that they are much larger than our 3% scale uncertainty. Limited information for the $\mathcal{O}(a^2)$ accurate twisted mass action can be extracted from the results for the ρ meson mass given in Ref. [65]. In this study of the hadronic vacuum polarization contribution to $(g-2)_\mu$, the correlators for vector mesons are calculated only using a one-particle interpolator for several ensembles with different lattice spacings and (larger-than-physical) pion masses. The mass of the ρ is then found by treating it as a stable particle and the results obtained show no significant dependence on the lattice spacing. We therefore assume that the 3% scale uncertainty and the 10% larger-than-physical pion mass are dominant systematics but we cannot exclude other sources of error, in particular lattice spacing effects or the omission of the strange quark from the sea.

In Figs. 7 and 8 we compare our results on the ρ meson mass and coupling to those of other lattice studies that were carried out at larger pion masses. The coupling $g_{\rho\pi\pi}$ appears to be remarkably independent of the quark mass and also robust against other systematics.

Future work will extend the present study to $N_f = 2+1$ flavor configurations, including several lattice spacings, to enable a continuum-limit extrapolation. Working close to the physical pion mass is particularly valuable for simulations of scattering processes involving states that are near to thresholds, e.g., $X(3872)$ and $D\bar{D}^*$ or $D_{s0}(2317)$ and DK, where the gap relative to the threshold strongly depends on the light quark mass.

ACKNOWLEDGMENTS

This work was supported by the Deutsche Forschungsgemeinschaft grant SFB/TRR 55. The authors gratefully acknowledge the Gauss Centre for Supercomputing e.V. (http://www.gauss-center.eu) for granting computer time on SuperMUC at Leibniz Supercomputing Centre (LRZ, http://www.lrz.de) for this project. The CHROMA [66] software package was used, along with the locally deflated domain decomposition solver implementation of OPENQCD [67]. The ensembles were generated primarily on the SFB/TRR 55 QPACE computer [68,69], using BQCD [70]. G. S. B. and S. C. acknowledge the hospitality of the Mainz Institute for Theoretical Physics (MITP) where a significant portion of this article was completed. We thank Simone Gutzwiller [71] and Tommy Burch for preparatory work, Andrei Alexandru for discussion and Benjamin Gläßle for software support.

[1] M. Lüscher, Two particle states on a torus and their relation to the scattering matrix, Nucl. Phys. **B354**, 531 (1991).
[2] M. Lüscher, Volume dependence of the energy spectrum in massive quantum field theories. 2. Scattering states, Commun. Math. Phys. **105**, 153 (1986).
[3] K. Rummukainen and S. A. Gottlieb, Resonance scattering phase shifts on a non-rest frame lattice, Nucl. Phys. **B450**, 397 (1995).
[4] C. Kim, C. T. Sachrajda, and S. R. Sharpe, Finite-volume effects for two-hadron states in moving frames, Nucl. Phys. **B727**, 218 (2005).
[5] N. H. Christ, C. Kim, and T. Yamazaki, Finite volume corrections to the two-particle decay of states with non-zero momentum, Phys. Rev. D **72**, 114506 (2005).
[6] X. Feng, K. Jansen, and D. B. Renner, Resonance parameters of the ρ-meson from lattice QCD, Phys. Rev. D **83**, 094505 (2011).
[7] Z. Davoudi and M. J. Savage, Improving the volume dependence of two-body binding energies calculated with lattice QCD, Phys. Rev. D **84**, 114502 (2011).
[8] Z. Fu, Rummukainen-Gottlieb's formula on two-particle system with different mass, Phys. Rev. D **85**, 014506 (2012).

[9] L. Leskovec and S. Prelovsek, Scattering phase shifts for two particles of different mass and non-zero total momentum in lattice QCD, Phys. Rev. D **85**, 114507 (2012).

[10] M. Göckeler, R. Horsley, M. Lage, U.-G. Meißner, P. E. L. Rakow, A. Rusetsky, G. Schierholz, and J. M. Zanotti, enquoteScattering phases for meson and baryon resonances on general moving-frame lattices, Phys. Rev. D **86**, 094513 (2012).

[11] S. Aoki *et al.* (CP-PACS Collaboration), Lattice QCD calculation of the rho meson decay width, Phys. Rev. D **76**, 094506 (2007).

[12] J. Frison *et al.* (BMW-c Collaboration), Rho decay width from the lattice, *Proc. Sci.*, LATTICE2010 (2010) 139, arXiv:1011.3413.

[13] C. B. Lang, D. Mohler, S. Prelovsek, and M. Vidmar, Coupled channel analysis of the rho meson decay in lattice QCD, Phys. Rev. D **84**, 054503 (2011); **89**, 059903(E) (2014).

[14] S. Aoki *et al.* (PACS-CS Collaboration), ρ meson decay in $2+1$ flavor lattice QCD, Phys. Rev. D **84**, 094505 (2011).

[15] C. Pelissier and A. Alexandru, Resonance parameters of the rho-meson from asymmetrical lattices, Phys. Rev. D **87**, 014503 (2013).

[16] J. J. Dudek, R. G. Edwards, and C. E. Thomas (Hadron Spectrum Collaboration), Energy dependence of the ρ resonance in $\pi\pi$ elastic scattering from lattice QCD, Phys. Rev. D **87**, 034505 (2013); **90**, 099902(E) (2014).

[17] B. Fahy, J. Bulava, B. Hörz, K. J. Juge, C. Morningstar, and C. H. Wong, Pion-pion scattering phase shifts with the stochastic LapH method, *Proc. Sci.*, LATTICE2014 (2014) 077, arXiv:1410.8843.

[18] D. J. Wilson, R. A. Briceño, J. J. Dudek, R. G. Edwards, and C. E. Thomas, Coupled $\pi\pi$, $K\bar{K}$ scattering in P-wave and the ρ resonance from lattice QCD, Phys. Rev. D **92**, 094502 (2015).

[19] J. Bulava, B. Hörz, B. Fahy, K. J. Juge, C. Morningstar, and C. H. Wong, Pion-pion scattering and the timelike pion form factor from $N_{\mathrm{f}}=2+1$ Lattice QCD simulations using the stochastic LapH method, in Proceedings of 33rd International Symposium on Lattice Field Theory, Kobe, 14–18 July, 2015 (to be published), arXiv:1511.02351.

[20] D. Guo and A. Alexandru, Resonance parameters for the rho-meson from lattice QCD, in Proceedings of 33rd International Symposium on Lattice Field Theory, Kobe, 14–18 July, 2015 (to be published), arXiv:1511.06334.

[21] Z. Fu and K. Fu, Lattice QCD study on $K^*(892)$ meson decay width, Phys. Rev. D **86**, 094507 (2012).

[22] S. Prelovsek, L. Leskovec, C. B. Lang, and D. Mohler, K π scattering and the K^* decay width from lattice QCD, Phys. Rev. D **88**, 054508 (2013).

[23] J. J. Dudek, R. G. Edwards, C. E. Thomas, and D. J. Wilson (Hadron Spectrum Collaboration), Resonances in coupled $\pi K - \eta K$ scattering from quantum chromodynamics, Phys. Rev. Lett. **113**, 182001 (2014).

[24] D. J. Wilson, J. J. Dudek, R. G. Edwards, and C. E. Thomas, Resonances in coupled πK, ηK scattering from lattice QCD, Phys. Rev. D **91**, 054008 (2015).

[25] K. A. Olive (Particle Data Group), Review of particle physics, Chin. Phys. C **38**, 090001 (2014).

[26] R. R. Akhmetshin *et al.* (CMD-2 Collaboration), Cross-section of the reaction $e^+e^- \to \pi^+\pi^-\pi^+\pi^-$ below 1 GeV at CMD-2, Phys. Lett. B **475**, 190 (2000).

[27] M. N. Achasov *et al.*, Study of the process $e^+e^- \to \pi^+\pi^-\pi^0$ in the energy region $\sqrt{s}$ below 0.98 GeV, Phys. Rev. D **68**, 052006 (2003).

[28] B. Jongejans *et al.* (Amsterdam-CERN-Nijmegen-Oxford Collaboration), Rare decay modes of $K^*(1420)$ and $K^*(892)$, Nucl. Phys. **B139**, 383 (1978).

[29] D. Aston *et al.*, The strange meson resonances observed in the reaction $K^- p \to \bar{K}^0\pi^+\pi^- n$ at 11 GeV/c, Nucl. Phys. **B292**, 693 (1987).

[30] G. S. Bali, S. Collins, B. Gläßle, M. Göckeler, J. Najjar, R. H. Rödl, A. Schäfer, R. W. Schiel, W. Söldner, and A. Sternbeck, Nucleon isovector couplings from $N_f = 2$ lattice QCD, Phys. Rev. D **91**, 054501 (2015).

[31] G. S. Bali *et al.* (QCDSF Collaboration), Nucleon mass and sigma term from Lattice QCD with two light fermion flavors, Nucl. Phys. **B866**, 1 (2013).

[32] G. S. Bali, S. Collins, B. Gläßle, M. Göckeler, J. Najjar, R. H. Rödl, A. Schäfer, R. W. Schiel, A. Sternbeck, and W. Söldner, The moment $\langle x \rangle_{u-d}$ of the nucleon from $N_f = 2$ lattice QCD down to nearly physical quark masses, Phys. Rev. D **90**, 074510 (2014).

[33] G. S. Bali *et al.* (QCDSF Collaboration), The strange and light quark contributions to the nucleon mass from lattice QCD, Phys. Rev. D **85**, 054502 (2012).

[34] M. Albaladejo, G. Ríos, J. A. Oller, and L. Roca, Finite volume treatment of $\pi\pi$ scattering in the ρ channel, arXiv:1307.5169.

[35] S. Kreuzer and H.-W. Hammer, On the modification of the Efimov spectrum in a finite cubic box, Eur. Phys. J. A **43**, 229 (2010).

[36] R. A. Briceño and Z. Davoudi, Three-particle scattering amplitudes from a finite volume formalism, Phys. Rev. D **87**, 094507 (2013).

[37] M. T. Hansen and S. R. Sharpe, Relativistic, model-independent, three-particle quantization condition, Phys. Rev. D **90**, 116003 (2014).

[38] U.-G. Meißner, G. Ríos, and A. Rusetsky, Spectrum of three-body bound states in a finite volume, Phys. Rev. Lett. **114**, 091602 (2015).

[39] M. T. Hansen and S. R. Sharpe, Expressing the three-particle finite-volume spectrum in terms of the three-to-three scattering amplitude, Phys. Rev. D **92**, 114509 (2015).

[40] S. Güsken, U. Löw, K.-H. Mütter, R. Sommer, A. Patel, and K. Schilling, Nonsinglet axial vector couplings of the baryon octet in lattice QCD, Phys. Lett. B **227**, 266 (1989).

[41] M. Falcioni, M. L. Paciello, G. Parisi, and B. Taglienti (APE Collaboration), Again on SU(3) glueball mass, Nucl. Phys. **B251**, 624 (1985).

[42] M. Hamermesh, *Group theory and its application to physical problems* (Addison-Wesley, Reading, MA, 1962).

[43] C. Michael, Adjoint sources in Lattice Gauge Theory, Nucl. Phys. **B259**, 58 (1985).

[44] M. Lüscher and U. Wolff, How to calculate the elastic scattering matrix in two-dimensional Quantum Field Theories by numerical simulation, Nucl. Phys. **B339**, 222 (1990).

[45] B. Blossier, M. Della Morte, G. von Hippel, T. Mendes, and R. Sommer, On the generalized eigenvalue method for energies and matrix elements in lattice field theory, J. High Energy Phys. 04 (2009) 094.

[46] H. Burkhardt, *Dispersion relation dynamics: A phenomenological introduction to S-matrix theory* (North-Holland, Amsterdam, 1969).

[47] D. R. Bolton, R. A. Briceño, and D. J. Wilson, Connecting physical resonant amplitudes and lattice QCD, arXiv:1507.07928.

[48] F. von Hippel and C. Quigg, Centrifugal-barrier effects in resonance partial decay widths, shapes, and production amplitudes, Phys. Rev. D **5**, 624 (1972).

[49] Z. Li, M. Guidry, T. Barnes, and E. S. Swanson, $I = 0, 1$ $\pi\pi$ and $I = 1/2$ $K\pi$ scattering using quark Born diagrams, arXiv:hep-ph/9401326.

[50] J. R. Peláez and F. J. Yndurain, The pion-pion scattering amplitude, Phys. Rev. D **71**, 074016 (2005).

[51] C. McNeile, C. Michael, and P. Pennanen (UKQCD Collaboration), Hybrid meson decay from the lattice, Phys. Rev. D **65**, 094505 (2002).

[52] C. McNeile and C. Michael (UKQCD Collaboration), Hadronic decay of a vector meson from the lattice, Phys. Lett. B **556**, 177 (2003).

[53] S. A. Gottlieb, P. B. Mackenzie, H. B. Thacker, and D. Weingarten, The $\rho - \pi\pi$ coupling constant in lattice gauge theory, Phys. Lett. B **134**, 346 (1984).

[54] S. A. Gottlieb, P. B. MacKenzie, H. B. Thacker, and D. Weingarten, Hadronic couplings constants in lattice gauge theory, Nucl. Phys. **B263**, 704 (1986).

[55] C. Alexandrou, J. W. Negele, M. Petschlies, A. Strelchenko, and A. Tsapalis, Determination of Δ resonance parameters from lattice QCD, Phys. Rev. D **88**, 031501 (2013).

[56] C. Hanhart, J. R. Peláez, and G. Ríos, Quark mass dependence of the rho and sigma from dispersion relations and chiral perturbation theory, Phys. Rev. Lett. **100**, 152001 (2008).

[57] J. R. Peláez and G. Ríos, Chiral extrapolation of light resonances from one and two-loop unitarized chiral perturbation theory versus lattice results, Phys. Rev. D **82**, 114002 (2010).

[58] K. Kawarabayashi and M. Suzuki, Partially conserved axial vector current and the decays of vector mesons, Phys. Rev. Lett. **16**, 255 (1966).

[59] Riazuddin and Fayyazuddin, Algebra of current components and decay widths of rho and K^* mesons, Phys. Rev. **147**, 1071 (1966).

[60] M. Peardon, J. Bulava, J. Foley, C. Morningstar, J. Dudek, R. G. Edwards, B. Joó, H.-W. Lin, D. G. Richards, and K. J. Juge (Hadron Spectrum Collaboration), A novel quark-field creation operator construction for hadronic physics in Lattice QCD, Phys. Rev. D **80**, 054506 (2009).

[61] C. Morningstar, J. Bulava, J. Foley, K. J. Juge, D. Lenkner, M. Peardon, and C. H. Wong, Improved stochastic estimation of quark propagation with Laplacian Heaviside smearing in Lattice QCD, Phys. Rev. D **83**, 114505 (2011).

[62] D. Mohler, C. B. Lang, L. Leskovec, S. Prelovsek, and R. M. Woloshyn, $D^*_{s0}(2317)$ meson and D-meson-kaon scattering from Lattice QCD, Phys. Rev. Lett. **111**, 222001 (2013).

[63] C. B. Lang, L. Leskovec, D. Mohler, S. Prelovsek, and R. M. Woloshyn, D_s mesons with DK and D^*K scattering near threshold, Phys. Rev. D **90**, 034510 (2014).

[64] C. B. Lang, D. Mohler, S. Prelovsek, and R. M. Woloshyn, Predicting positive parity B_s mesons from lattice QCD, Phys. Lett. B **750**, 17 (2015).

[65] F. Burger, X. Feng, G. Hotzel, K. Jansen, M. Petschlies, and D. B. Renner (ETM Collaboration), Four-flavor leading-order hadronic contribution to the muon anomalous magnetic moment, J. High Energy Phys. 02 (2014) 099.

[66] R. G. Edwards and B. Joó (SciDAC, LHPC and UKQCD Collaborations), The Chroma software system for Lattice QCD, Nucl. Phys. B, Proc. Suppl. **140**, 832 (2005).

[67] http://luscher.web.cern.ch/luscher/openQCD/.

[68] H. Baier *et al.*, QPACE: A QCD parallel computer based on Cell processors, *Proc. Sci.*, LAT2009 (2009) 001, arXiv:0911.2174.

[69] Y. Nakamura, A. Nobile, D. Pleiter, H. Simma, T. Streuer, T. Wettig, and F. Winter, Lattice QCD applications on QPACE, Procedia Computer Science **4**, 841 (2011).

[70] Y. Nakamura and H. Stüben, BQCD-Berlin quantum chromodynamics program, Proc. Sci., LATTICE2010 (**2010**) 040 [arXiv:1011.0199].

[71] S. Gutzwiller, Scattering phase shift for elastic two pion scattering and the rho resonance in Lattice QCD, Ph.D thesis, Universität Regensburg (2012).